Theoretical Study on the Structures and Absorption Properties of Yellow Azomethine Dyes

Seiji Ichijima,* Hiroo Fukunaga, Hidetoshi Kobayashi, Makoto Ishihara, and Nobuaki Koga[†]

Ashigara Research Laboratories, Fuji Photo Film Co., Ltd., Kanagawa 250-0193

[†]Graduate School of Human Informatics, Nagoya University, Nagoya 464-8601

(Received September 27, 2002)

To examine the relationship between the structural features and the visible absorption spectra of yellow α-acylacetanilide azomethine dyes, we carried out measurements of the visible absorption spectra, X-ray crystal structure analyses, and density functional theory calculations for 2-benzoyl-2-[*N*-(4-diethylamino-2-methylphenyl)imino]-2′-chloroacetanilide (BA) and 2-[*N*-(4-diethylamino-2-methylphenyl)imino]-2-pivaloyl-2′-chloroacetanilide (PA). BA shows a visible absorption spectrum, which has a relatively high molar extinction coefficient and an unwanted absorption curve in the green region, while PA shows a visible absorption spectrum, which has a relatively low molar extinction coefficient and a sharp cut absorption curve in the green region. BA and PA have a common structural feature that the *p*-aminophenyl fragment is coplanar with the azomethine-carbamoyl (–N=C–CONH–) fragment, resulting in a chromophore, but is perpendicular to the acyl fragment. The stable structures are dominated by the effect of π-conjugation in the chromophore moiety and a repulsive interaction between the *p*-aminophenyl fragment and the acyl fragment. The potential energy curve for the rotation of the *p*-aminophenyl fragment shows two minima, and suggests that in BA two conformations coexist in equilibrium, while PA takes only single conformation in equilibrium. The difference in the absorption spectra of BA and PA is mainly attributed to the number of conformers coexisting in equilibrium.

Azomethine dyes are known to be among the most important dyes, because of their wide applications, including color photographic systems, dye diffusion thermal transfer (D2T2) print systems, and others.[1] Due to the central roles as image dyes, they have been the subjects of considerable research interest to obtain guiding principles for molecular design.[2–7] To elucidate the absorption properties of azomethine dyes, theoretical calculations on geometry as well as absorption properties are of crucial importance because of flexibility in the geometry and the strong dependence of absorption properties on it.

In the color photographic systems, yellow azomethine dyes are formed during the developing process by the oxidative coupling reactions of 4-(dialkylamino)anilines with α-acylacetanilides.

Good color reproducibility and good optical image sharpness are demanded for the yellow-image dyes used in color photographic systems. To realize good color reproducibility, it is needed that the absorption spectrum of a yellow dye has a sharp-cut curve in the green region. In addition, as the extinction coefficient in the blue absorption band for a yellow dye increases, the light-sensitive layer coated on a film can be thinned by reducing the amount of α-acylacetanilide required to produce a given density. As a result, unwanted image smear caused by light scattering decreases, and the optical image becomes sharper.

The α-acylacetanilide azomethine dyes have been improved for use in photographic systems since the pioneering work by Brown et al. about 40 years ago.[8] In the present color photographic systems, two yellow azomethine dyes derived from 2-benzoyl-2′-chloroacetanilide (hereafter referred to as BA) and 2-pivaloyl-2′-chloroacetanilide (hereafter referred to as PA) have been used extensively. The chemical structures of these two dyes are shown in Fig. 1.

However, these two dyes are not optimum candidates as yellow image dyes from the point of view of the visible absorption spectra. Though the molar extinction coefficient in the blue absorption band of BA is relatively high, the unwanted absorption is seen in the green region (500–550 nm). On the other hand, the absorption spectrum of PA has a sharper-cut curve in the green region than that of BA, while the molar extinction coefficient for the blue band of PA is relatively small. To find new dyes that show the desirable absorption spectra, it is required to elucidate why the absorption spectra of the two dyes are different. For a thorough understanding of the absorption characteristics, we examine here the relationship between the structural features and the visible

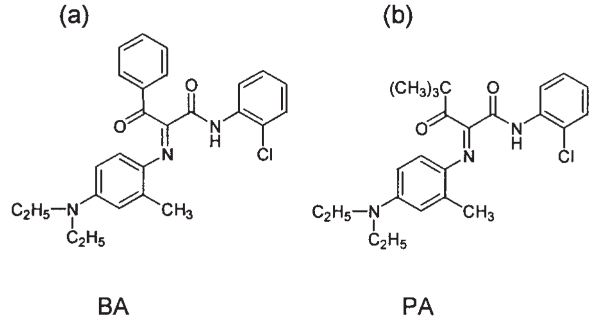

Fig. 1. Chemical structures for the α-acylacetanilide azomethine dyes of (a) 2-benzoyl-2-[*N*-(4-diethylamino-2-methylphenyl)imino]-2′-chloroacetanilide (BA) and (b) 2-[*N*-(4-diethylamino-2-methylphenyl)imino]-2-pivaloyl-2′-chloroacetanilide (PA).

absorption spectra of BA and PA both experimentally and theoretically.

Several theoretical and experimental investigations on the structures and the absorption spectra of azomethine dyes have been performed over the past decade. Nakamura et al.[2] examined the torsion dependence of the absorption spectra for indoaniline dyes, which are widely used as cyan image dyes. Using the structures obtained both by the X-ray crystal structure analysis and by the molecular orbital (MO) calculations with the AM1 method,[9] the absorption wavelengths and their intensities were calculated by the INDO/S method.[10] It is stated that the decrease in the degree of planarity brings about a red shift and a lowering of the absorption intensity in the longest transition. Friedrich et al.[4] compared the structures and the absorption wavelengths calculated for the azomethine dyes with the several semi-empirical MO methods. They reported that the AM1 method predicts the bond lengths and the bond angles within the statistical error, but gives incorrect torsion angles for flexible molecules, such as α-acylacetanilide azomethine dyes. In addition, it is reported that the INDO/S method is the most useful for evaluating the absorption wavelengths among the semi-empirical MO methods, when an accurate geometry of the dye is given. We determined the molecular structures crystallographically for a series of α-acylacetanilide azomethine dyes.[5] In the molecular structures, the p-aminophenyl fragment is coplanar with the azomethine-carbamoyl fragment, but perpendicular to the acyl fragment. Daiba et al.[6] examined the molar extinction coefficients of α-acylacetanilide azomethine dyes. Using the structures obtained by combining the Monte-Carlo method and molecular orbital calculations at the AM1 level, the absorption wavelengths and their intensities were calculated by the INDO/S method. Abu-Hasanayn et al.[7] carried out geometry optimization for some α-acylacetanilide azomethine dyes both in the ground state and in the lowest triplet state. The geometry obtained for the BA type dye in the ground state agrees with the crystallographically determined molecular structure.

To analyze the difference in the absorption spectra of BA and PA, it is required to obtain accurate geometries and potential energy curves for some flexible torsion. We used the density functional theory (DFT) method to obtain structural information for BA and PA, since high accuracy is needed to take into account the subtle balance between the stability induced by π-conjugation and the steric repulsion, which is realized by ab intio MO calculations.[11] The absorption wavelengths and their intensities for the two dyes must also be calculated quantitatively. Among the ab initio MO methods, the time-dependent density functional theory (TD-DFT) method with the Becke's hybrid exchange functional (B3)[12] and the Lee–Yang–Parr correlation functional (LYP)[13] gives the vertical excitation energies in the visible region most accurately.[14] The TD-DFT method is also applicable to relatively large molecules because of an effective consideration of the electron correlation effects and a great reduction of the computation expense.[15] In addition, for calculating the absorption wavelengths for dyes that are important in the field of the dye industry, the TD-DFT method is more accurate than the INDO/S method.[16]

In the present article, we examine the stable geometries of BA and PA both crystallographically and theoretically. We also calculate the potential energy curves for some torsions and the absorption spectra using density functional methods. From these results we clarify the reason for the difference in the absorption spectra of BA and PA.

Method

Preparation. Figure 1 shows the chemical structures of the sample azomethine dyes of 2-benzoyl-2-[*N*-(4-diethylamino-2-methylphenyl)imino]-2′-chloroacetanilide (BA) and 2-[*N*-(4-diethylamino-2-methylphenyl)imino]-2-pivaloyl-2′-chloroacetanilide (PA). Using a procedure reported by Brown et al.,[8] BA and PA were synthesized by oxidative coupling reactions of 4-diethylamino-2-methylaniline with 2-benzoyl-2′-chloroacetanilide and 2-pivaloyl-2′-chloroacetanilide, respectively, in which ammonium peroxodisulfate was used as the oxidizing agent.

Measurement of the Ultraviolet and Visible Absorption Spectra. These two dyes were diluted with ethyl acetate in the spectrum grade made in Wako Chemical Co. Ltd. to prepare solution samples of 2×10^{-5} M (1 M = 1 mol dm^{-3}), respectively. The ultraviolet and visible absorption spectra of the samples were recorded with a 1cm cell using a Shimadzu Automatic Recording Spectrophotometer (UV260).

X-ray Crystal Structure Analysis. Single crystals of BA and PA were obtained by recrystallization from acetonitrile and methanol, respectively. Diffraction data were collected at room temperature using an Enraf–Nonius CAD-4 four-circle diffractometer with graphite-monochromated Cu Kα radiation ($\lambda = 0.154184$ nm). The structures were solved using the program package SHELXS86.[17] All positions of non-hydrogen atoms were determined from an E-map and refined by a full-matrix least squares method with anisotropic thermal parameters. All of the hydrogen atoms were placed at idealized positions and refined as riding atoms with the relative isotropic parameters.

Molecular Orbital Calculations. To obtain the most stable geometries for BA and PA, we performed ab initio MO calculations at the three levels: (1) the Hartree–Fock method with the 3-21G basis set[18] (HF/3-21G), (2) the Hartree–Fock method with the 6-31G basis set[19] augmented with a set of d-type polarization functions (HF/6-31G(d)), and (3) the DFT method with the Becke's nonlocal three-parameter hybrid exchange functional (B3) in conjunction with the Lee-Yang-Parr correlation functional (LYP) with the polarized split-valence shell 6-31G(d) basis set (B3LYP/6-31G(d)).[20] First, using the crystallographically determined structures as the initial structures, geometry optimization was carried out with the HF/3-21G method. In the initial structures, the bond lengths associated with the hydrogen atoms were corrected by the standard values while the bond angles and the torsion angles are kept invariant, since the positions of the hydrogen atoms cannot be determined exactly by the X-ray crystal structure analysis. Then, the structures obtained by the HF/3-21G method were used as the initial structures in a successive geometry optimization with the HF/6-31G(d) method, and so on.

Using the B3LYP/6-31G(d) method, we also calculated the potential energy curves for the torsion angles (t3, t5, and t6), defined in Fig. 2. In these calculations, all of the geometrical parameters were optimized at every 10° of t5 or every 20° of t3 or t6.

Furthermore, using the optimized geometries obtained for the two dyes with the B3LYP/6-31G(d) method, the lower energy vertical excitations and the corresponding intensities were calculated with the time-dependent density functional theory (TD-DFT) method[14] using the B3 exchange functional with the LYP correlation functional with the 6-31G(d) basis set. All of the above-mentioned calculations were performed using the Gaussian98[21] packages.

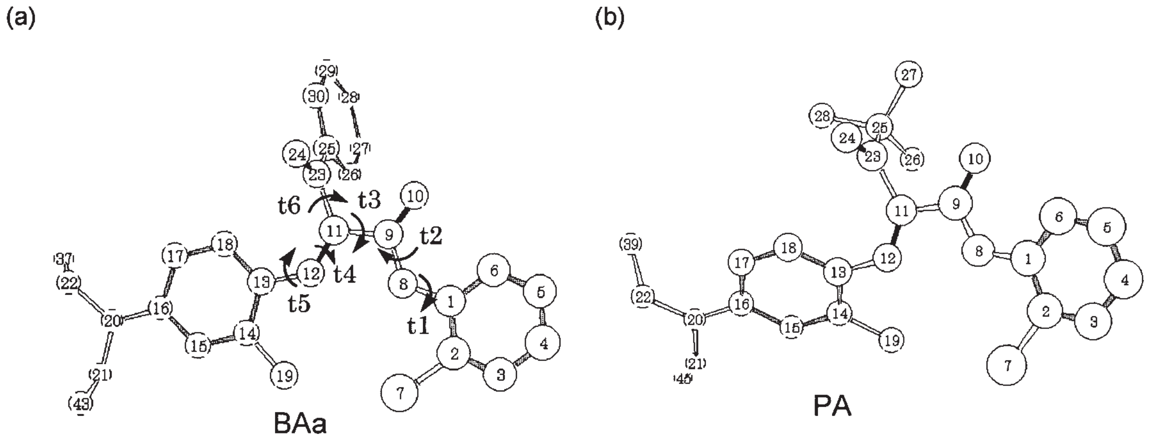

Fig. 2. Crystallographically determined molecular structures of (a) BAa and (b) PA. Numerical values indicate the atom numbering. For BA, torsion angles of t1 to t6 are also defined in the Fig., and the definition of t1 to t6 for PA is similar to BA.

Results and Discussion

1. Structural Features. Crystallographically Determined Molecular Structure: Table 1 summarizes the crystal data and the final results of the refinements for BA and PA. BA crystallized to give a mixture of two kinds of polymorphism: one is a monoclinic crystal that includes only a single conformation (hereafter referred to as BAa), and the other is a triclinic crystal that consists of two kinds of conformations (hereafter referred to as BAb and BAc, respectively). On the other hand, PA crystallized to give a triclinic crystal possessing only a single conformation.

Figure 2 shows the crystallographically determined molecular structures of BAa and PA together with the atom numbering, and Table 2 indicates the geometrical parameters in all of the molecular structures obtained for BA and PA. The torsion angles listed in Table 2 are defined in Fig. 2. In all of the molecular structures of BA and PA, the *p*-aminophenyl fragment is coplanar with the azomethine-carbamoyl fragment, but is perpendicular to the acyl fragment. Comparing the three structures of BAa, BAb and BAc, we can see a prominent difference in the torsion angles t5 and t6, as given in Table 2. Judging from the signs of t5 and t6, the three molecular structures of BA are classified into two types: one has a negative value in t5 and a positive value in t6 (BAa), and the other has a positive value in t5 and a negative value in t6 (BAb and BAc), whose absolute values vary around 0° and 90°, respectively. It is mentioned in passing that the structure of PA is similar to that of BAa from the point of view of the signs of t5 and t6. However, in PA, the torsion angle t1 largely deviates from 180° because of the packing effect in the crystal, in contrast to BA. Thus, the crystallographically determined molecular structures suggest a difference in the flexibility of twist around some rotatable bonds between BA and PA. To understand the flexibility difference, information on the potential-energy curves for the related torsion angles is required.

Table 1. Crystal Data and Results of Refinement

	BA		PA
Crystal data			
Chemical formula	$C_{26}H_{26}$ Cl N_3O_2		$C_{24}H_{30}$ Cl N_3O_2
Chemical formula weight	448.0		428.0
Cell setting	Monoclinic	Triclinic	Triclinic
Space group	$P2_1/n$	$P\bar{1}$	$P\bar{1}$
a/Å	13.249	15.590	11.006
b/Å	8.296	11.139	10.966
c/Å	22.397	14.990	11.876
α/°	90	102.70	114.23
β/°	107.08	113.34	112.59
γ/°	90	76.53	71.93
V/Å^3	2253.2	2353.6	1186.9
Z	4	4	2
Temperature/K	297	296	298
$D_{\rm calc}$ /g cm^3	1.264	1.293	1.197
Crystal form	Prismatic	Prismatic	Prismatic
Crystal color	Yellow	Dark orange	Yellow
Refinement			
R-factor	0.061	0.058	0.069
No. of reflections	3540	7095	3393
No. of parameters	289	577	271

Optimized Geometry: Table 2 indicates the geometrical parameters of the equilibrium structures obtained at the three levels of ab initio MO calculations. We obtained two structures for BA, starting from the three initial structures mentioned in Method. Since the geometrical parameters of these two structures are almost the same, except for the signs of torsion angles t5 and t6, they are mirror images of each other, and therefore only the geometrical parameters of the structure obtained from the BAa initial structure are given in Table 2.

First, we discuss the dependence of the structure of BA on the computational methods. It can be found from Table 2 that the N(8)–C(9), C(9)–C(10), C(11)–N(12), and C(11)–C(23) bond lengths in the B3LYP/6-31G(d) structure are longer than those of the structures by the other methods. In the chromophore moiety, the HF/3-21G method and the HF/6-31G(d) method give a structure with the highest planarity and the most twisted structure, respectively. The torsion angle t5 deviates least from 0° using the HF/3-21G method as the result of overestimation of the stability induced by the π-conjugation. The HF/6-31G(d) method gives a largely distorted structure to avoid a steric repulsion. The most reliable B3LYP/6-31G(d) method gives a structure in which the stability induced by the π-conjugation is suitably balanced by the

Table 2. Selected Geometrical Parameters in the Structures Obtained by the X-ray Crystal Structure Analysis and the Ab Initio MO Calculations[a]

Geometrical parameters	BA							PA				
	Exptl[b]			Calcd				Exptl[b]	Calcd			
	BAa	BAb	BAc	HF /3-21G[c]	HF /6-31G*[c]	B3LYP /6-31G*[c]	B3LYP /6-31G*[d]		HF /3-21G[c]	HF /6-31G*[c]	B3LYP /6-31G*[c]	B3LYP /6-31G*[d]
Bond length												
C(1)–N(8)	1.401	1.390	1.401	1.394	1.399	1.397	1.397	1.410	1.395	1.400	1.398	1.398
N(8)–C(9)	1.358	1.329	1.341	1.352	1.351	1.370	1.371	1.344	1.348	1.349	1.367	1.368
C(9)–O(10)	1.213	1.216	1.203	1.219	1.199	1.228	1.229	1.223	1.223	1.201	1.231	1.231
C(9)–C(11)	1.501	1.492	1.498	1.504	1.516	1.509	1.508	1.502	1.505	1.517	1.508	1.512
C(11)–N(12)	1.276	1.274	1.273	1.256	1.251	1.283	1.285	1.270	1.255	1.250	1.282	1.284
C(11)–C(23)	1.521	1.496	1.504	1.512	1.528	1.532	1.534	1.534	1.514	1.533	1.537	1.544
N(12)–C(13)	1.394	1.389	1.393	1.409	1.412	1.397	1.394	1.406	1.411	1.413	1.398	1.394
C(16)–N(20)	1.371	1.365	1.366	1.374	1.380	1.383	1.381	1.376	1.377	1.383	1.385	1.385
Non-bond distance												
Cl(7)–HN(8)				2.495	2.475	2.488	2.492		2.493	2.476	2.488	2.486
N(12)–HN(8)				2.172	2.208	2.166	2.162		2.153	2.198	2.159	2.123
Bond angle												
C(9)–C(11)–N(12)	117.5	119.1	118.5	119.1	118.9	118.8	118.5	117.2	118.4	118.5	118.4	117.1
C(9)–C(11)–C(23)	112.2	111.6	111.9	111.4	112.9	112.9	113.4	112.8	112.0	112.9	112.7	115.5
N(12)–C(11)–C(23)	130.3	129.3	129.7	129.5	128.2	128.3	127.6	129.5	129.6	128.7	128.8	126.6
C(11)–N(12)–C(13)	129.9	128.4	129.3	130.2	125.9	127.2	127.1	125.7	130.5	125.9	127.8	127.2
Torsion angle												
t1: C(2)–C(1)–N(8)–C(9)	173.9	177.1	177.8	180.0	−175.7	−178.8	−179.6	−147.8	−179.7	−174.3	−178.9	−179.2
t2: C(1)–N(8)–C(9)–C(11)	176.5	176.5	175.8	−179.7	178.5	178.7	−179.0	175.7	−179.7	178.6	179.1	−178.8
t3: N(8)–C(9)–C(11)–N(12)	−4.6	0.7	2.3	−0.4	−9.3	−5.2	3.9	−3.4	−2.7	−8.6	−6.0	6.0
t4: C(9)–C(11)–N(12)–C(13)	−179.5	179.6	179	178.1	−179.5	178.7	−178.7	177.2	177.8	−180.0	178.6	−179.2
t5: C(11)–N(12)–C(13)–C(18)	−4.8	18.7	3.5	−27.0	−43.8	−34.2	28.0	−37.1	−31.9	−47.8	−36.1	36.3
t6: N(12)–C(11)–C(23)–O(24)	90.5	−99.1	−89.5	82.6	94.5	91.3	67.0	98.5	74.9	88.3	84.3	58.8

a) Distances and angles are in Å unit and degree unit, respectively. b) The geometrical parameters in the crystallographically determined structures are shown. c) The values shown in this column are calculated for the global minimum structure. d) The values shown in this column are calculated for the local minimum structure.

repulsive interactions acting on crowded atoms.

Further, it is required to ascertain whether the aforementioned equilibrium structures obtained for the two dyes are the most stable or not. Though a complete conformational analysis with high-quality calculations is needed to search for the global minimum, we cannot execute such calculations because of many rotatable bonds. Alternatively, we performed geometry optimization with the B3LYP/6-31G(d) method for the rotamer of three single bonds around the double bond C(11)–N(12) in both dyes. As a result, we could not find any more stable structures than the aforementioned equilibrium structures. Considering these situations, it is concluded that the equilibrium structures derived from the crystallographically determined structures are the global minima for both dyes.

We next discuss the structures obtained for BA and PA by the B3LYP/6-31G(d) method. Judging from the distance between the polar hydrogen atoms and the heteroatoms, we can recognize the two hydrogen bonds for both dyes. One is a weak hydrogen bond of Cl(7)···HN(8) and the other is a strong hydrogen bond of N(12)···HN(8). The N(12)···HN(8) hydrogen bond restricts the twist motion around the C(9)–C(11) bond, resulting in a planar chromophore moiety with twisting of the acyl fragment. It should also be noted that the torsion angle, t5 in BA is almost the same as that in PA, though the torsion angle t6 depends on the acyl fragment. The details are discussed in a later section.

Potential Energy Curves: Figure 3 shows a comparison between PA and BA in the potential energy curve for the torsion around t3. It is found from Fig. 3 that both of the potential energy curves are relatively steep and almost coincident with each other, since the potential energy curves are dominated by the π-conjugation energy in the chromophore moiety.

Figure 4 shows the potential energy curves for torsion angle t6 for PA and BA. In contrast to the case for t3, the potential energy curve for t6 in PA is steeper than that in BA over the whole range of t6. This is caused by the fact that the acyl phenyl group of BA and the acyl *t*-butyl group of PA comes into contact with the *p*-aminophenyl fragment and the azomethine-carbamoyl fragment by twisting the acyl fragment clockwise (in the direction of larger t6) and anticlockwise (in the direction of smaller t6), respectively.

Figure 5 shows a comparison between PA and BA in the potential energy curve scanned over a wide range of t5. As shown in Fig. 5, the potential energy curves of BA and PA coincide with each other in the range of t5 from −90° to −40°, while they are very different in the range of t5 from −40° to 90°. The *p*-aminophenyl fragment comes into contact with the acyl fragment by the twists around the N(12)–C(13) bond. The twist in the direction of smaller t5 (−40° to −90°) brings about contact between the hydrogen atom C(18)H and the oxygen atom O(24). Such a repulsive interaction does not depend very much on the size and shape of the acyl fragment, resulting in similar potential energy curves in the range of t5 from −90° to −40° between BA and PA. On the other hand, with the twist in the opposite direction, the *p*-aminophenyl fragment gets close to the acyl phenyl group in BA, and to the acyl *t*-butyl group in PA. The size and shape of the acyl fragment apparently determine the degree of congestion, and thus affect the shape of the potential energy curves in this larger range of t5.

We can also see the two minima in both potential energy curves for torsion angle t5 obtained for BA and PA, as shown in Fig. 5. To examine the energetic and structural details in the local minima, we carried out full geometry optimization with the B3LYP/6-31G(d) method, starting from the local minimum structures obtained in calculations of the potential energy curves. The thus-obtained structures for BA and PA have energies of 1.7 and 8.4 kJ/mol, respectively, relative to each global minimum—the relative energies do not include zero-point energy (ZPE) corrections. The geometrical parameters of the two local minima are indicated in Table 2, which shows that t6 largely deviates

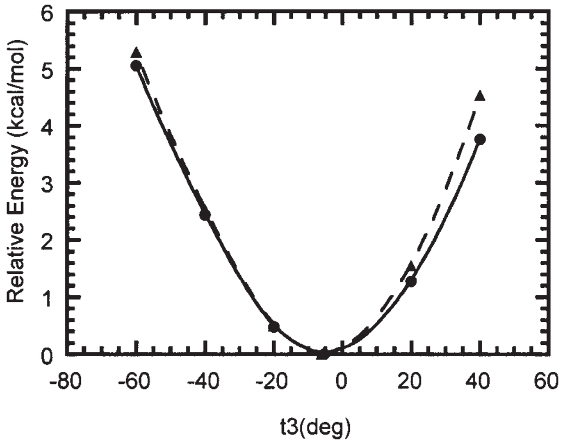

Fig. 3. Potential energy curves for the torsion angle t3 of BA (solid line) and PA (dashed line).

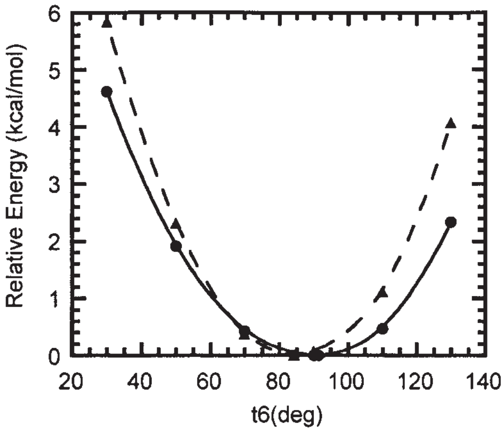

Fig. 4. Potential energy curves for the torsion angle t6 of BA (solid line) and PA (dashed line).

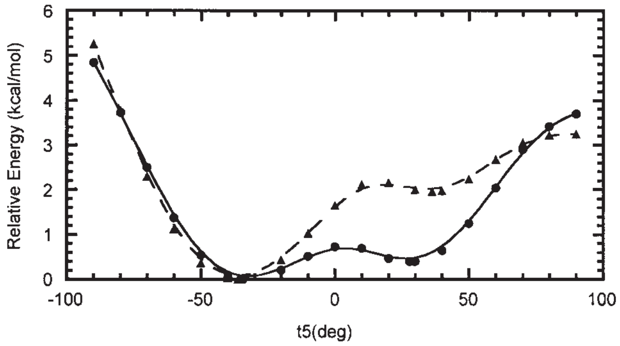

Fig. 5. Potential energy curves for the torsion angle t5 of BA (solid line) and PA (dashed line).

from 90° in the BA and PA local minima, though the deviation in the PA local minimum is larger than that in the BA local minimum because of the larger repulsive interaction between the *p*-aminophenyl fragment and the *t*-butyl group of the acyl fragment. In addition, t5 in the local minimum of BA is smaller than that of PA, leading to an increase in the stability induced by the π-conjugation in BA. Thus, the stabilities of the local minima are dominated by the strength of the π-conjugation in the chromophore moiety and the repulsive interaction between the *p*-aminophenyl and acyl fragments.

2. Absorption Spectra. **Observed Absorption Spectra:** Figure 6 shows a comparison between BA and PA in the observed ultraviolet and visible absorption spectra, and Table 3 indicates the numerical values for the peak wavelengths and their molar extinction coefficients. It is found from Fig. 6 and Table 3 that the first peaks locate around 440 nm in both dyes, resulting in a yellow color, though the peak wavelength for BA is longer by 2 nm than that for PA. It is also found that the molar extinction coefficient in the main absorption band of BA is larger than that of PA, and the long-wavelength tail (500–550 nm) of the main absorption band for BA is larger than that for PA. In addition, we analyzed the main absorption band with a deconvolution scheme using Gaussian functions, and show the results in Fig. 6 and Table 3. The main absorption band in BA was divided into two components; one component has a peak located at 437 nm (major component), and the other at 456 nm (minor component). The ratio of the area for the minor component to the major component is 0.20. On the other hand, the main absorption band in PA was fitted by only one component.

Comparison of the Observed and Calculated Absorption Spectra: Table 3 gives the calculated excitation energies and the oscillator strengths for the lower energy transitions using the global and local minimum structures as well as the experimental excitation energies and intensities. As indicated in Table 3, the observed absorption wavelengths in the lower energy transitions for both BA and PA were reproduced quantitatively by calculations with the global minimum structures, while the ratio of the absorption intensities for the minor component to the major component calculated for BA is largely different from the experimental one. The ratio of the absorption intensities calculated for BA with the local minimum structure is also not in agreement with the observed one, though the two observed absorption wavelengths could be reproduced using the local minimum structure.

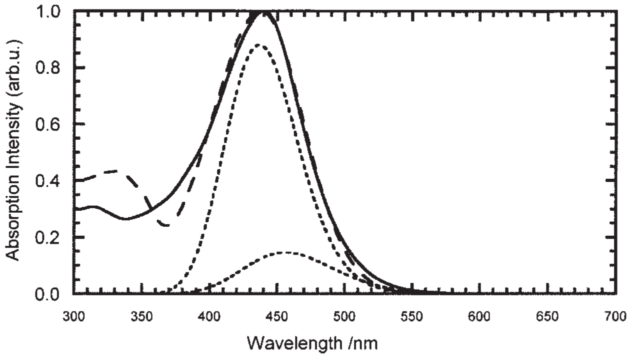

Fig. 6. Visible absorption spectra observed in ethyl acetate solution of 2×10^{-5} M for BA (solid line) and PA (dashed line). The absorption spectra (dotted line) obtained by a deconvolution scheme with Gaussian functions are also shown.

As mentioned above, from the relative energies of the local minimum structure to the global minimum structure, it is considered that both conformers coexist in equilibrium for BA, while only the single conformer exists for PA. By averaging the two excitation energies calculated for the global and local minima of BA based on the canonical distribution at room temperature, the intensity ratio of the minor component to the major component becomes 0.28, which is comparable to the experimental one (0.20). In addition, the ratio of the absorption intensity summed up for the bands in the range of 400–450 nm for BA to that for PA is estimated to be 1.18, which is in good agreement with the experimental one (1.25). Thus, the observed visible absorption spectrum of BA comes from the superposition of the absorption energy transitions for the two conformers.

Assignment of the Calculated Transition: Table 4 indicates the dominant configurations for the lower energy transitions obtained with the global minimum structures by TD-DFT calculations. Figure 7 shows the molecular orbitals (MO's) related to the dominant configurations for BA. Both the lowest and second energy transitions of BA, which have different oscillator strengths from each other, are assigned to the π–π^* transition, as shown in Table 4 and Fig. 7. The difference in the intensities is because of the overlap density between the occupied MO and the unoccupied MO associated with the transition, as follows. In the first transition, the 118th MO (highest occupied molecular orbital; HOMO) delocalizes on the chromophore

Table 3. Absorption Wavelengths (nm) and Intensities[a]

Band	BA				PA		
	Calcd[b]	Calcd[c]	Exptl[d]	Exptl[e]	Calcd[b]	Calcd[c]	Exptl[d]
1	448.7	444.1		456		456.5	
	0.003	0.292		3300		0.351	
2	429.9	402.3	440	437	435.5		438
	0.445	0.204	20000	16700	0.391		16000
3	353.7	376.9	340–380		360.7	378.0	340–360
	0.121	0.157	< 5000		0.170	0.154	< 5000

a) Upper and lower values stand for the absorption wavelengths and their intensities, respectively. The calculated intensities correspond to the oscillator strength, and the observed ones correspond to the molar extinction coefficients. b) Calculated for the global minimum structure. c) Calculated for the local minimum structure. d) Measured for the ethyl acetate solution of 2×10^{-5} M. e) obtained by a deconvolution scheme with Gaussian functions.

Table 4. Main Configuration and Its Weight for the Lower Energy Transitions[a)]

Transition	BA				PA			
	Global minimum		Local minimum		Global minimum		Local minimum	
1	118 → 120	46%	118 → 119	35%			114 → 115	37%
2	118 → 119	37%	118 → 120	40%	114 → 115	38%		
3	116 → 119	29%	116 → 119	34%	112 → 115	37%	112 → 115	33%

a) Only configurations with the weight over 10% are shown in the table.

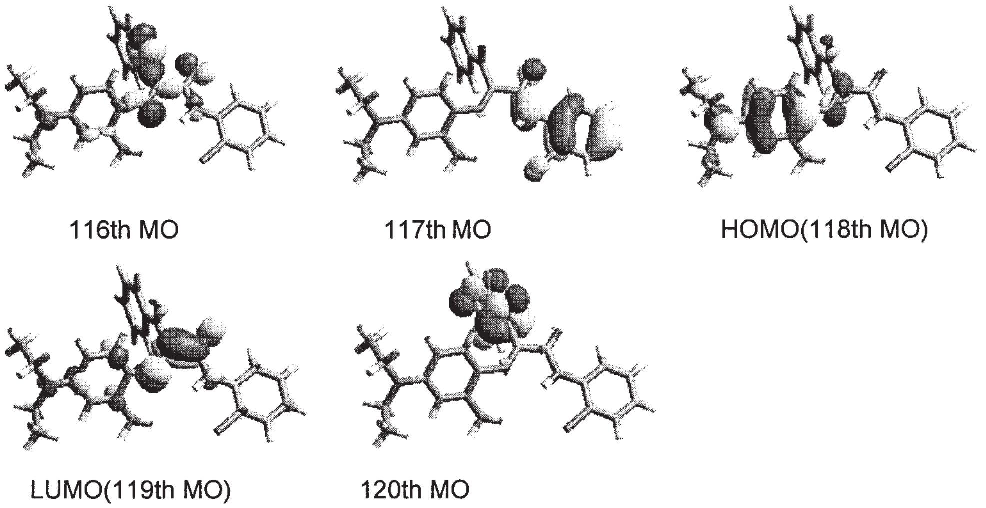

Fig. 7. Molecular orbitals obtained for BA in the global minimum.

plane, and the 120th MO localizes in the phenyl ring perpendicular to the chromophore plane, resulting in a negligible overlap density. In the second transition, both the 118th MO and the 119th MO (lowest unoccupied molecular orbital; LUMO) delocalize on the chromophore plane, and therefore the overlap density is larger. On the other hand, in the 116th MO associated with the third transition, the lone-pair orbitals of the nitrogen atom N(12) and the oxygen atoms O(10) and O(24) interact with the π orbital delocalizing on the p-aminophenyl fragment, leading to a smaller overlap density and, in turn, to a smaller intensity. Since the 112th to 116th MO's for PA (not shown) are similar to the 116th to 120th MO's for BA, respectively, the first and second transitions for PA correspond to the second and third transitions in BA, respectively. The first transition in BA is unique, and relates to the unwanted behavior of the curve in the green region.

Torsion Angle Dependence of the Main Absorption Band: To examine the dependence of the visible absorption spectra on the torsion angles, we calculated the excitation energies at structures with different torsion angles. The structures were generated by the following procedure. First, we optimized the ideal structure with fixing t6 to be 90°, and the other torsion angles, except for the alkyl groups, to be 0° or 180°. Second, one of the t3, t5, and t6 in the ideal structure was changed by ±20° or ±40°, and we optimized the structure while fixing the selected torsion angle at the changed value and the other torsion angles at the same values in the ideal structure. Using the thus-generated geometries, we performed TD-DFT calculations of the excitation energies for the rotational isomers of BA. Figure 8 shows the torsion-angle dependence of the absorption wavelengths and the oscillator strengths. Table 5 indicates the dominant configurations for each excited state.

The twist of t3 around 0° causes a blue shift in the main transition while keeping the corresponding intensity almost constant. This transition is assigned to the HOMO–LUMO excitation, though the energy levels of the 119th MO and the 120th MO (HOMO) are inverted in the structure with $t3 = 40°$. The twist of t3 raises the energy of LUMO due to the in-phase combination between C(9) and C(11), and increases the HOMO–LUMO energy gap while keeping the overlap density between them.

The twist of t6 around 90° causes a red shift in the main transition. The red shift is attributed to a decrease in the energy of LUMO due to an in-phase interaction induced by the twist. On the whole, the intensity for the transition becomes smaller with a twist of t6 around 90°. In LUMO of the rotational isomer with t6 of 90° and 0°, the p-aminophenyl π system conjugates to the azomethine-carbamoyl and the acyl π systems, respectively. In the intermediate values between 0° and 90° for t6, it conjugates to both π systems with the ratio of the degree of conjugation depending on the value of t6. Therefore, the complicated behavior of the intensity dependence on t6 comes from a change of the π-conjugation.

The twist of t5 around 0° causes the red shift in the main transition. In contrast to indoaniline dyes,[2] in the α-acylacetanilide azomethine dyes, the red shift is caused by the facts that HOMO is destabilized by the twist of t5 with keeping the energy level of LUMO almost constant and that the HOMO and LUMO orbitals localize on p-aminophenyl and azomethine-carbamoyl fragments, respectively, the excitation being of charge-transfer character. The decrease in the intensity is simply due to the decrease in the overlap density between HOMO and LUMO.

In BA, the largest oscillator strength, 0.63, is estimated for the

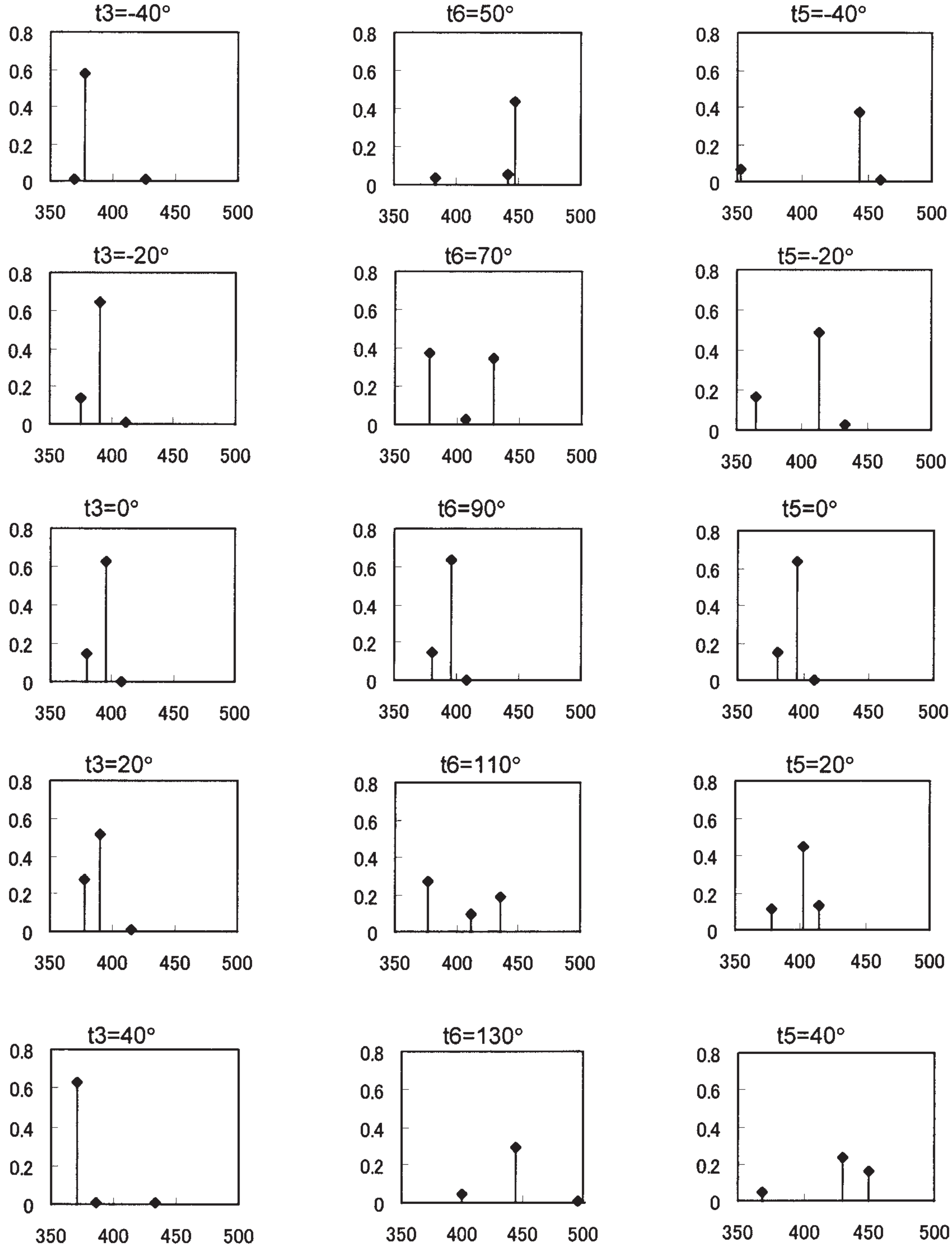

Fig. 8. Transitions obtained for the rotational isomers of t3, t5, and t6. The vertical axis and horizontal axis indicate the oscillator strength and the absorption wavelength (nm), respectively.

main transition of the ideal rotational isomer (t3 = 0°, t5 = 0°, and t6 = 90°), while the oscillator strength calculated for the global minimum (t3 = −5°, t5 = −34°, and t6 = 91°) becomes 0.45. The decrease in the oscillator strength mainly comes from the twist of t5. As indicated in Table 3, PA has a smaller oscillator strength for the main transition in the global minimum (t3 = −6°, t5 = −36°, and t6 = 84°) than BA. This is almost attributed to the twist of t6. Comparing the global minimum structure (t3 = −5°, t5 = −34°, and t6 = 91°) with the local minimum structure (t3 = 4°, t5 = 28°, and t6 = 67°) in BA, we can see a large difference in t6. Hence, it is found that the drastic decrease of the oscillator strength in the local minimum is mainly caused by the twist of t6.

The question to address now is how we can rationally design yellow azomethine dyes with a higher absorption intensity in the blue region and a lower absorption intensity in the green region. Since the loss of the absorption intensity for BA and PA in the global minimum is mainly due to the deviations of t5 and t6 from 0° and 90°, respectively, the first strategy needed to explore novel

Table 5. Main Configurations for the Lower Energy Transitions Calculated for Various Structures of BA[a)]

Torsion angle	Transition 1	Transition 2	Transition 3
t3			
−40°	25% (118 → 119), 23% (118 → 120)	16% (118 → 119), 17% (118 → 120)	27% (116 → 119), 12% (117 → 119)
−20°	46% (118 → 120)	33% (118 → 119)	33% (116 → 119)
0°	47% (118 → 120)	32% (118 → 119)	40% (116 → 119)
20°	47% (118 → 120)	27% (118 → 119)	33% (116 → 119), 11% (118 → 119)
40°	42% (118 → 119)	26% (116 → 119), 16% (117 → 119)	26% (118 → 120)
t5			
−40°	44% (118 → 120)	37% (118 → 119)	24% (116 → 119), 15% (116 → 120)
−20°	40% (118 → 120)	29% (118 → 119)	34% (116 → 119)
0°	47% (118 → 120)	32% (118 → 119)	40% (116 → 119)
20°	32% (118 → 120), 14% (118 → 119)	21% (118 → 119), 16% (118 → 120)	35% (116 → 119)
40°	32% (118 → 119), 13% (118 → 120)	35% (118 → 120)	31% (116 → 119)
t6			
50°	34% (118 → 119)	40% (116 → 119)	43% (117 → 119)
70°	35% (118 → 119)	43% (116 → 119)	34% (118 → 120)
90°	47% (118 → 120)	32% (118 → 119)	40% (116 → 119)
110°	27% (118 → 119)	34% (116 → 119)	25% (118 → 120), 18% (117 → 119)
130°	36% (116 → 119)	36% (118 → 119)	39% (117 → 119)

a) Only configurations with the weight over 10% are shown in the table.

dyes is to make the deviation smaller. The second strategy is to increase the energy difference between the global and local minima, so that the problem of a minor component with a red-shifted wavelength can become small.

In comparison between BA and PA, a benzoyl group is proper for designing t6 to 90°, since a bulkier acyl fragment, such as a pivaloyl group, causes the deviation of t6 from 90° in the global minimum. However, a proper bulky acyl fragment is appropriate for increasing the energy difference between the global and local minima because of the larger deviation of t6 from 90° in the local minimum. Although it is not easy to arrange a compromise between these demands for the acyl fragment, the selection of the proper acyl fragment in size and shape between the benzoyl and pivaloyl groups would approach a solution to the question.

Conclusions

We examined the structural features of BA and PA both experimentally and theoretically. BA and PA have common features in crystallographically determined structures and MO-derived structures, i.e. the *p*-aminophenyl fragment is coplanar with the azomethine-carbamoyl fragment, but is perpendicular to the acyl fragment. These structures are characterized by three torsion angles of (t3, t5, and t6). Compared to the structural features between BA and PA, a prominent difference can be recognized in the potential energy curves for t5. In both BA and PA, two minima, which have different signs for t5 with each other, were found. The energy difference between the two minima is only 1.7 kJ/mol in BA, resulting in the coexistence of the two conformations in equilibrium. On the other hand, PA takes only the single conformation in equilibrium.

To clarify the difference in the absorption spectra of BA and PA, we carried out TD-DFT calculations for the equilibrium structures as well as the rotational isomers. It is found that the loss of the absorption intensity is dominated by the twist of t5 and t6. The intensity of the observed main band in BA is lager than that in PA. This is due to the difference in t6, which depends on the shape and size in the acyl fragment. Since the absorption intensity for BA in the global minimum structure is smaller than that in the ideal isomer ($t3 = 0°$, $t5 = 0°$, and $t6 = 90°$), we could improve the α-acylacetanilide azomethine dye regarding the absorption intensity.

Furthermore, BA shows a visible absorption spectrum with unwanted absorption in the green region. The longer transition comes from the characteristic transition of BA from the π orbital delocalized on the chromophore moiety to the π^* orbital localized in the phenyl group of the acyl fragment. In addition, the absorption spectrum of BA is represented by the superposition of the two absorption energy transitions derived from the global and local minima, since the two conformations coexists in equilibrium. The absorption band derived from the local minimum mainly contributes to the first transition corresponding to the green region. Therefore the unwanted absorption in the green region in BA is caused by the high flexibility of t5.

References

1 For review articles, a) R. D. Theys and G. Sosnovsky, *Chem. Rev.*, **97**, 83 (1997). b) R. Bradbury, “Advances in Color Chemistry Series 3, (Modern Colorants: Synthesis and Structures),” (1995), p. 154.

2 M. Adachi, Y. Murata, and S. Nakamura, *J. Am. Chem. Soc.*, **115**, 4331 (1993).

3 M. Adachi and Y. Murata, *J. Phys. Chem. A*, **102**, 841 (1998).

4 L. E. Friedrich and J. E. Eilers, *J. Imaging Sci. and Tech.*, **38**, 24 (1994).

5 a) N. Saito and S. Ichijima, Presented at the International Symposium on Silver Halide Imaging, 1997. b) H. Kobayashi, K. Yamada, Y. Yoshioka, H. Fukunaga, S. Ichijima, and K. Ogawa, Presented at the International Congress of Photographic Science

Meeting, Belgium, 1998.

6 S. Daiba, T. Oshiyama, and F. Ishii, *J. Soc. Photogr. Sci. Tech. Japan*, **62**, 371 (1999).

7 F. Abu-Hasanayn and W. G. Herkstroeter, *J. Phys. Chem. A*, **105**, 1214 (2001).

8 G. H. Brown, J. Figueras, R. J. Gledhill, C. J. Kibler, F. C. McRossen, S. M. Parmerter, P. W. Vittum, and A. Weissberger, *J. Am. Chem. Soc.*, **79**, 2919 (1957).

9 M. J. S. Dewar, E. G. Zoebisch, E. F. Healy, and J. J. P. Stewart, *J. Am. Chem. Soc.*, **107**, 3902 (1985).

10 a) J. E. Ridley and M. C. Zerner, *Theor. Chim. Acta*, **32**, 111 (1973). b) A. D. Bacon and M. C. Zerner, *Theor. Chim. Acta*, **53**, 21 (1979). c) M. C. Zerner, G. H. Loew, R. F. Kirchner, and U. T. Mueller-Westerhoff, *J. Am. Chem. Soc.*, **102**, 589 (1980).

11 a) N. DiCesare, M. Belletete, C. Marrano, M. Leclerc, and G. Durocher, *J. Phys. Chem. A*, **102**, 5142 (1998). b) H. Guo and M. Karplus, *THEOCHEM*, **92**, 347 (1992). c) J. Cioslowski, P. Piskorz, G. Liu, and D. Moncrieff, *J. Phys. Chem.*, **100**, 19333 (1996). d) A. Goller and U. W. Grummt, *Chem. Phys. Lett.*, **321**, 399 (2000).

12 A. D. Becke, *J. Chem. Phys.*, **98**, 1372 (1993).

13 C. Lee, W. Yang, and R. G. Parr, *Phys. Rev. B*, **37**, 785 (1988).

14 a) R. Bauernschmitt and R. Ahlrichs, *Chem. Phys. Lett.*, **256**, 454 (1996). b) M. E. Casida, C. Jamorski, K. C. Casida, and D. R. Salahub, *J. Chem. Phys.*, **108**, 4439 (1998). c) C. Jamorski, M. E. Casida, and D. R. Salahub, *J. Chem. Phys.*, **104**, 5134 (1996). d) R. E. Stratmann, G. E. Scuseria, and M. J. Frisch, *J. Chem. Phys.*, **109**, 8218 (1998).

15 a) C. Muguruma, N. Koga, Y. Hatanaka, I. El-Sayed, M. Mikami, and M. Tanaka, *J. Phys. Chem. A*, **104**, 4928 (2000). b) J. Danielsson, J. Ulin, and A. Laaksonen, *J. Am. Chem. Soc.*, **123**, 9817 (2001). c) N. Matsuzawa, A. Ishitani, D. A. Dixon, and T. Uda, *J. Phys. Chem. A*, **105**, 4953 (2001). d) J. L. Weisman and M. H. Gordon, *J. Am. Chem. Soc.*, **123**, 11686 (2001). e) R. Bauernschmitt, R. Ahlrichs, F. H. Hennrich, and M. M. Kappes, *J. Am. Chem. Soc.*, **120**, 5052 (1998).

16 D. Guillaumont and S. Nakamura, *Dyes and Pigments*, **46**, 85 (2000).

17 G. M. Sheldrick, *Acta Crystallogr.*, **A46**, 467 (1990).

18 J. S. Binkley, J. A. Pople, and W. J. Hehre, *J. Am. Chem. Soc.*, **102**, 939 (1980).

19 P. C. Hariharan and J. A. Pople, *Theor. Chim. Acta.*, **28**, 213 (1973).

20 A. D. Becke, “Density-functional thermochemistry. Ⅲ. The role of exact exchange,” *J. Chem. Phys.*, **98**, 5648 (1993).

21 M. J. Frisch, G. W. Trucks, H. B. Schlegel, G. E. Scuseria, M. A. Robb, J. R. Cheeseman, V. G. Zakrzewski, J. A. Montgomery, Jr., R. E. Stratmann, J. C. Burant, S. Dapprich, J. M. Millam, A. D. Daniels, K. N. Kudin, M. C. Strain, O. Farkas, J. Tomasi, V. Barone, M. Cossi, R. Cammi, B. Mennucci, C. Pomelli, C. Adamo, S. Clifford, J. Ochterski, G. A. Petersson, P. Y. Ayala, Q. Cui, K. Morokuma, D. K. Malick, A. D. Rabuck, K. Raghavachari, J. B. Foresman, J. Cioslowski, J. V. Ortiz, A. G. Baboul, B. B. Stefanov, G. Liu, A. Liashenko, P. Piskorz, I. Komaromi, R. Gomperts, R. L. Martin, D. J. Fox, T. Keith, M. A. Al-Laham, C. Y. Peng, A. Nanayakkara, M. Challacombe, P. M. W. Gill, B. Johnson, W. Chen, M. W. Wong, J. L. Andres, C. Gonzalez, M. Head-Gordon, E. S. Replogle, and J. A. Pople, “Gaussian 98, Revision A.7,” Gaussian Inc., Pittsburgh, PA (1998).